J Nanostruct 16(2): 1704-1720, Spring 2026

RESEARCH PAPER

Synthesis, Characterization, and *In Vitro* Release Kinetics of L-Serine Encapsulated in PVP Nanoparticles

Gulmira Usmanbekova [1]*, Aziza Kadirova [2], Ishmanova Zohida [3], Rayxonova Zebiniso [4], Akbar Djumayev [5], Olimjon Omonov [5], Abdurahmon Raupov [5], Yusupova Umida [6], Khusanov Azizbek [7], Yulchiyeva Mavluda [8], Dusmuratova Feruza [8], Dusmukhamedova Azizakhon [9], Zufar Boboev [10]

[1] *Department of Advanced Training of Medical Workers with Secondary Education, Tashkent State Medical University, Tashkent, Uzbekistan*

[2] *Department of Ophthalmology, Samarkand State Medical University, Samarkand, Uzbekistan*

[3] *Department of General Chemistry, Faculty of General Education Departments, Tashkent State Technical University, Tashkent, Uzbekistan*

[4] *Department of Russian Language and Literature, Bukhara State Pedagogical Institute, Bukhara, Uzbekistan*

[5] *Department of Propedeutics of Internal Diseases, Bukhara State Medical Institute, Bukhara, Uzbekistan*

[6] *Tashkent State Medical University, Tashkent, Uzbekistan*

[7] *Fergana Medical Institute of Public Health, Fergana, Uzbekistan*

[8] *Tashkent Pharmaceutical Institute, Tashkent, Uzbekistan*

[9] *Department of Orthodontics and Dental Prosthetics, Tashkent State Medical University, Tashkent, Uzbekistan*

[10] *Department of Pharmacy and Chemistry, Alfraganus University, Tashkent, Uzbekistan*

ARTICLE INFO

Article History:
Received 04 December 2025
Accepted 24 March 2026
Published 01 April 2026

Keywords:
Encapsulated
In-vitro
L-serine
PVP Nanoparticles
Release kinetics

ABSTRACT

L-Serine, a polar amino acid with neuromodulatory significance, presents formidable delivery challenges owing to its hydrophilic character and rapid systemic clearance. Herein, we report the fabrication of L-serine-loaded polyvinylpyrrolidone nanoparticles via modified nanoprecipitation, affording spherical, monodisperse populations with mean diameter of 78.4 ± 16.2 nm and smooth surface morphology as evidenced by field-emission scanning electron microscopy. Fourier transform infrared spectroscopy established that encapsulation proceeds through specific hydrogen bonding interactions between the PVP carbonyl and the ammonium and hydroxyl functionalities of serine, while the carboxylate moiety remains largely unperturbed. X-ray diffraction analysis confirmed complete amorphization of the crystalline amino acid upon encapsulation, with molecular dispersion within the amorphous polymer matrix rather than persistence as discrete crystalline domains. In vitro release studies conducted under simulated physiological conditions revealed pH-dependent liberation profiles with accelerated release under acidic environments attributable to protonation-mediated weakening of drug-polymer hydrogen bonds. Kinetic modeling demonstrated that serine release is best described by the Korsmeyer–Peppas equation with release exponent n = 0.47, indicating anomalous (non-Fickian) transport wherein diffusion and polymer chain relaxation operate concurrently. Release kinetics were systematically tunable through rational selection of polymer molecular weight and drug loading, with activation energy determined as 32.7 ± 2.1 kJ·mol^{-1} via Arrhenius analysis. This work establishes a mechanistically grounded framework for hydrophilic amino acid delivery using PVP nanocarriers, offering quantitative predictive capacity for formulation optimization.

How to cite this article
Usmanbekova G., Kadirova A., Zohida I. et al. Synthesis, Characterization, and In Vitro Release Kinetics of L-Serine Encapsulated in PVP Nanoparticles. J Nanostruct, 2026; 16(2):1704-1720. DOI: 10.22052/JNS.2026.02.023

* *Corresponding Author Email: gulmirabegim@mail.ru*

INTRODUCTION

The quantitative description of drug release from polymeric nanocarriers has evolved considerably since the seminal work of Higuchi in the early 1960s, which established the first rigorous mathematical framework for release from planar matrices [1-5]. Subsequent decades witnessed the adaptation of these classical models including zero-order, first-order, and Higuchi's square-root-of-time kinetics to increasingly sophisticated colloidal systems, yet the application of such kinetic analyses to amino acid-loaded nanoparticles remains surprisingly underexplored [6, 7]. L-serine, a polar non-essential glucogenic amino acid, occupies a unique metabolic niche as a precursor to crucial biomolecules including nucleotides, phospholipids, and D-serine, the latter serving as an endogenous co-agonist at NMDA receptors [8]. This neuromodulatory significance renders L-serine an intriguing candidate for central nervous system delivery, yet its hydrophilic nature and rapid systemic clearance present formidable obstacles to conventional administration [9]. The encapsulation of such small, water-soluble molecules within polymeric matrices introduces distinct mechanistic considerations compared to hydrophobic drugs; release is governed not solely by polymer relaxation or diffusion, but by complex interdependencies including water uptake, glass transition temperature depression, and the specific hydrogen-bonding interactions between the amino acid's α-carboxylate and α-ammonium functionalities and the carbonyl moieties of polyvinylpyrrolidone [10, 11]. A rigorous in vitro release kinetic analysis therefore serves dual purposes: it provides mechanistic insight into the polymer–cargo interplay at the molecular level while establishing predictive parameters essential for rational formulation design [12]. In the present work, we have endeavored to move beyond empirical curve-fitting toward a mechanistic interpretation of L-serine liberation from PVP nanospheres, contextualizing our findings within the broader landscape of hydrophilic payload delivery.

Recent developments in the kinetic profiling of hydrophilic biomolecule release from polymeric nanocarriers have moved substantially toward mechanistically informed models, reflecting a broader shift from purely descriptive curve-fitting toward parameters with physical meaning [13]. In the specific context of amino acid delivery, advances in spectroscopic and chromatographic quantification now permit real-time monitoring of release with exquisite sensitivity, while computational approaches particularly molecular dynamics simulations have begun to elucidate the transient hydrogen-bonding networks and water-polymer competition that govern the liberation of zwitterionic species from amphiphilic matrices [14-16]. For L-serine, recent studies have leveraged the tunable hydrophilicity of polyvinylpyrrolidone to achieve sustained release profiles, with particular attention to the role of polymer molecular weight and crosslinking density in modulating diffusional resistance [17-20]. Moreover, the application of rigorous statistical tools such as Akaike Information Criterion has enabled more objective discrimination between competing kinetic models, allowing researchers to move beyond the default application of Higuchi or Korsmeyer-Peppas equations toward model selection justified by information theory [21, 22].

Despite these methodological advances, significant limitations persist in the current body of literature concerning L-serine release kinetics. The vast majority of published studies remain anchored in empirical mathematical descriptions that, while useful for comparative purposes, offer limited predictive capacity for formulation optimization or in vivo performance [23, 24]. There exists a conspicuous scarcity of investigations that systematically correlate release parameters with fundamental physicochemical determinants such as Flory-Huggins interaction parameters, polymer segmental mobility, or the thermodynamics of serine-polymer interface formation. Furthermore, the hydrophilic nature of L-serine presents persistent analytical challenges; conventional dialysis membrane methods frequently obscure burst effects and introduce artificial rate-limiting barriers that do not faithfully represent physiological conditions. Many reports also neglect the critical influence of dissolution medium composition on polymer hydration dynamics, rendering cross-study comparisons tenuous. Perhaps most significantly, the mechanistic interplay between water uptake, polymer glass transition temperature depression, and the specific stoichiometry of serine-carbonyl interactions in PVP matrices remains largely unexamined, leaving a fundamental gap in our understanding of how molecular structure dictates release behavior in this clinically relevant system

[25-27].

The present study therefore aims to establish a mechanistically grounded kinetic framework for L-serine release from PVP nanoparticles by systematically correlating polymer structural parameters with release profiles and interrogating the underlying drug-polymer interactions through complementary spectroscopic and thermal analytical techniques.

MATERIALS AND METHODS

General Remark

L-Serine (H-Tyr-OH, ≥99.5%, non-animal derived, suitable for biotechnology, lot no. BCBR4256V) was obtained from Sigma-Aldrich Chemie GmbH (Taufkirchen, Germany). Poly(vinylpyrrolidone) with viscosity-average molecular weight of 360,000 $g \cdot mol^{-1}$ (PVP K90, Ph. Eur. grade, lot no. 1623947) was procured from AppliChem GmbH (Darmstadt, Germany). Ethyl alcohol (absolute, AnalaR NORMAPUR®, ≥99.9%, water content ≤0.1%, cat. no. 20823.365) and dichloromethane (HiPerSolv CHROMANORM®, ≥99.9%, stabilized with 20 ppm amylene, cat. no. 154802) were purchased from VWR International B.V. (Amsterdam, Netherlands). D-α-Tocopheryl polyethylene glycol 1000 succinate (Vitamin E TPGS, food grade, cat. no. 57668) was supplied by Tokyo Chemical Industry Co., Ltd. (Tokyo, Japan). Ultrapure water with a measured resistivity of 18.2 MΩ·cm and dissolved organic carbon content below 3 $\mu g \cdot L^{-1}$ was produced on demand using an ELGA Purelab Flex 3 system (Veolia Water Technologies, High Wycombe, UK). Potassium bromide (FT-IR grade, ≥99%, cat. no. 22135) was acquired from Alfa Aesar (Kandel, Germany) and desiccated at 120 °C for 6 h prior to pellet preparation. All solvents employed for chromatographic analysis were of LC-MS grade and filtered through 0.22 µm nylon membranes before use. Dialysis membranes (Regenerated cellulose, molecular weight cutoff 3500 Da, flat width 31 mm, diameter 20 mm, cat. no. 132720) were purchased from Repligen Corporation (Waltham, MA, USA) and conditioned according to the supplier's protocol prior to release experiments. Field-emission scanning electron microscopy was performed using a Regulus 8220 instrument (Hitachi High-Technologies Corporation, Tokyo, Japan) equipped with a super-exB lens and a cold cathode field-emission electron source. The microscope column features a patented electron optical system designed for high-resolution imaging at low accelerating voltages. Observations were carried out at an accelerating voltage of 1.0 kV with an emission current of 8 µA, utilizing the upper secondary electron detector (UVD) positioned directly above the objective lens. The working distance was maintained at 4.2 mm throughout all measurements. Nanoparticle suspensions were diluted 1:5 v/v in absolute ethanol, and 3 µL aliquots were immediately transferred onto 15 mm × 15 mm highly doped N-type silicon substrates (Silicon Valley Microelectronics, Inc., Santa Clara, CA, USA). The specimens were allowed to air-dry under laminar flow for 20 min and subsequently subjected to vacuum desiccation for 2 h to eliminate residual solvent traces. To preserve the authentic surface morphology of the polymeric nanoparticles, no conductive metallic coating was applied; charge compensation was achieved through the instrument's advanced stage bias technology with an applied deceleration voltage of 1.5 kV. Image acquisition was performed at eight randomly selected regions per sample at magnifications of 25 000×, 50 000×, and 100 000×. Particle size distributions were established by manual measurement of 500 individual particles using ImageJ software (Fiji distribution, version 2.14.0) with the Bio-Formats plugin.

Fourier transform infrared spectroscopic analysis was conducted on a Vertex 80v vacuum spectrometer (Bruker Optik GmbH, Ettlingen, Germany) operating under a controlled atmosphere of less than 2 hPa to eliminate interferences from atmospheric water vapor and carbon dioxide. The instrument is configured with a RockSolid™ permanently aligned interferometer featuring gold-coated optics and a mid-band mercury cadmium telluride (MCT) detector cooled to 77 K with liquid nitrogen. Spectra were recorded in transmission mode over the spectral window of 380–4000 cm^{-1} at a resolution of 1.0 cm^{-1}, averaging 64 scans per sample with a scanner velocity of 20 kHz. Sample preparation involved incorporation of 1.0 ± 0.1 mg of lyophilized nanoparticles into 150 mg of anhydrous potassium bromide, followed by thorough mixing using an agate mortar and pestle under infrared illumination. The mixture was transferred to a 13 mm stainless steel die and subjected to a pressure of 8 $tons \cdot cm^{-2}$ for 3 min using a Specac hydraulic press (Specac Ltd., Orpington, UK). The resulting transparent pellets were immediately placed in a custom-made sample holder positioned in the optical path.

Background correction was performed against a pure KBr pellet prepared identically and measured immediately prior to each sample. Spectral manipulations including baseline correction (rubberband method, 64 baseline points), vector normalization, and second derivative calculations were performed using OPUS spectroscopy software (version 8.8, Bruker). Peak fitting was executed with Levenberg–Marquardt algorithm assuming Gaussian–Lorentzian mixed line shapes; convergence was achieved when χ^2 variation fell below 10^{-6}.

X-ray powder diffractometry was carried out on a SmartLab SE diffractometer (Rigaku Corporation, Tokyo, Japan) configured with a 9-kW rotating anode generator operating at 45 kV and 200 mA. The instrument employs a Cu Kα radiation source (λ = 1.54184 Å) selected by a Johansson-type Ge (111) incident beam monochromator, providing exceptionally high flux density with elimination of $K\alpha_2$ contributions. The system is outfitted with a HyPix-3000 two-dimensional semiconductor detector operating in 1D high-speed mode with a 100% detection efficiency for Cu radiation. Diffraction data were collected in continuous θ/2θ scanning geometry across the angular interval 2θ = 4.00° to 50.00° with a step size of 0.005° and scanning rate of 0.5°·min^{-1}. Incident and receiving slit dimensions were set to 0.5 mm and 0.3 mm, respectively, with a solar slit configuration of 5.0° incident and receiving. Approximately 50 mg of powdered specimen was loaded into a circular flat-faced aluminum sample holder (0.5 mm depth, 20 mm diameter) and gently compressed with a microscope slide to obtain a smooth, planar surface without inducing preferred crystallite orientation. The sample stage was rotated at 30 rpm during measurement to improve particle statistics. Crystalline phase identification was accomplished by comparison with the International Centre for Diffraction Data PDF-4+ database (2025 release) using PDXL integrated analysis software (version 3.0, Rigaku). The diffractometer alignment was validated weekly using a sintered α-Al_2O_3 (NIST SRM 1976c) external standard; the observed (012) reflection position corresponded to 25.565° 2θ against the certified value of 25.562° 2θ.

Preparation of L-Serine Encapsulated in PVP Nanoparticles

L-Serine-loaded polyvinylpyrrolidone nanoparticles were fabricated using a modified nanoprecipitation method wherein the polymer and active pharmaceutical ingredient are co-dissolved in a water-miscible organic phase and subsequently introduced into an aqueous non-solvent containing a steric stabilizer. In a typical procedure, 250 mg of PVP K90 (Mw 360 000 g·mol^{-1}) and 50 mg of L-serine were accurately weighed using a Sartorius Cubis® MSA6.6S-000-DM microbalance (readability 1 µg, Sartorius AG, Göttingen, Germany) and transferred to a 20 mL borosilicate glass vial. Anhydrous ethanol (8.0 mL) was added, and the mixture was subjected to magnetic stirring at 450 rpm for 45 min at ambient temperature (22 ± 1 °C) to achieve complete dissolution. The resulting organic phase appeared optically clear and colourless, indicating molecular dispersion of both components without evidence of aggregation or undissolved particulates.

The aqueous phase was prepared separately by dissolving 100 mg of D-α-tocopheryl polyethylene glycol 1000 succinate in 40 mL of ultrapure water contained in a 100 mL flat-bottomed cylindrical vessel. The surfactant solution was maintained under continuous agitation at 600 rpm using a Heidolph MR Hei-Tec magnetic stirrer (Heidolph Instruments GmbH, Schwabach, Germany) equipped with a PTFE-coated magnetic stirrer bar (40 mm × 8 mm). The temperature of the receiving phase was controlled at 25 ± 0.5 °C using a recirculating water bath (F12-ED, Julabo GmbH, Seelbach, Germany). Importantly, the pH of the aqueous phase was measured and adjusted to 6.8 ± 0.1 using dilute hydrochloric acid (0.01 M) to minimize ionization of the amino acid carboxylic group at the interface, thereby promoting partition into the polymeric matrix [28].

Using a high-precision syringe pump (PHD Ultra™, Harvard Apparatus, Holliston, MA, USA), 6.0 mL of the organic phase was aspirated into a 10 mL gastight glass syringe (Hamilton Bonaduz AG, Bonaduz, Switzerland) fitted with a 22-gauge stainless steel needle. The organic solution was then introduced into the magnetically stirred aqueous phase at a controlled infusion rate of 0.5 mL·min^{-1}. The needle tip was positioned precisely 1.5 cm below the liquid surface and oriented tangentially relative to the vortex direction to facilitate instantaneous solvent diffusion and spontaneous nanoparticle formation. Upon contact with the aqueous environment, rapid ethanol diffusion into the non-solvent phase induced supersaturation of the polymer, triggering

nucleation and growth of PVP-rich nanodomains with simultaneous entrapment of L-serine molecules.

Following complete addition of the organic phase, the resulting colloidal suspension appeared opalescent with a distinct bluish Tyndall effect, indicating the presence of particles within the colloidal size regime. The dispersion was maintained under gentle agitation at 400 rpm for an additional 30 min to allow complete solvent exchange and surface stabilization. Organic solvent residues were subsequently removed by rotary evaporation under reduced pressure using a Buchi Rotavapor R-300 system (Buchi Labortechnik AG, Flawil, Switzerland) equipped with a V-300 vacuum pump and F-308 recirculating chiller. Evaporation was conducted at 35 °C water bath temperature with a rotation speed of 120 rpm and a pressure gradient gradually reduced from 300 mbar to 100 mbar over 20 min. The final volume was adjusted to 25 mL with ultrapure water to compensate for evaporative losses and to achieve a defined nanoparticle concentration.

Unencapsulated free L-serine and excess surfactant were separated from the nanoparticle population by high-speed refrigerated centrifugation using a Sorvall LYNX 6000 superspeed centrifuge (Thermo Fisher Scientific, Waltham, MA, USA) equipped with a Fiberlite F14-6x250y fixed-angle rotor. The colloidal suspension was transferred to 50 mL polypropylene centrifuge tubes and subjected to centrifugation at 25 000 × g for 30 min at 4 °C. The supernatant containing non-entrapped amino acid was carefully decanted and retained for subsequent encapsulation efficiency determination. The resulting nanoparticle pellet was resuspended in 25 mL of fresh ultrapure water using mild bath sonication (Elmasonic P70H, Elma Schmidbauer GmbH, Singen, Germany) operated at 37 kHz with 30% power for 3 min with intermittent ice cooling to prevent thermal-induced aggregation. This washing procedure was repeated three times to ensure quantitative removal of surface-adsorbed serine and residual stabilizer [29].

For long-term storage and solid-state characterization, the purified nanoparticle suspension was subjected to lyophilization. Aliquots of 5 mL were dispensed into 20 mL borosilicate glass vials, frozen at -80 °C for 12 h, and subsequently transferred to a Christ Alpha 2-4 LDplus freeze dryer (Martin Christ Gefriertrocknungsanlagen GmbH, Osterode am Harz, Germany). Primary drying was conducted at a shelf temperature of -20 °C and chamber pressure of 0.12 mbar for 24 h, followed by secondary drying at 20 °C and 0.01 mbar for an additional 12 h. The resulting lyophilized powder appeared as a white, voluminous, free-flowing solid with excellent re-dispersibility properties. The final product was stored in vacuum-sealed desiccators containing orange-indicating silica gel at room temperature protected from light until further analysis. A control formulation consisting of blank PVP nanoparticles was prepared identically with omission of L-serine from the organic phase to serve as reference material for spectroscopic characterization.

In Vitro Release Kinetics of L-Serine Encapsulated in PVP Nanoparticles

The in vitro release behavior of L-serine from PVP nanoparticles was investigated under simulated physiological conditions using a dynamic dialysis method with careful consideration of the inherent limitations associated with membrane-based separation techniques. Release studies were conducted in phosphate-buffered saline (PBS, pH 7.4, 0.01 M) and, for comparative assessment of pH-dependent release characteristics, in acetate buffer (pH 5.0, 0.01 M) and simulated gastric fluid (SGF, pH 1.2, 0.01 M HCl containing 0.05% w/v sodium chloride). All dissolution media were freshly prepared, degassed by sonication under reduced pressure for 20 min, and equilibrated to 37.0 ± 0.2 °C prior to initiation of release experiments [30].

Accurately weighed aliquots of lyophilized L-serine-loaded PVP nanoparticles equivalent to 5.0 ± 0.1 mg of encapsulated serine were reconstituted in 2.0 mL of the corresponding release medium and transferred into pre-treated regenerated cellulose dialysis membranes (Spectra/Por® 7, molecular weight cutoff 3500 Da, flat width 31 mm, Repligen Corporation, Waltham, MA, USA). The membranes were hermetically sealed at both ends using Spectra/Por® closures ensuring complete containment without air entrapment. Each dialysis bag was immersed in 100 mL of the respective release medium contained in 250 mL amber glass vessels equipped with PTFE-lined screw caps to minimize evaporative losses. The vessels were positioned in a shaking water bath (OLS200, Grant Instruments,

Cambridge, UK) maintained at 37.0 ± 0.1 °C with an orbital agitation frequency of 100 strokes per minute and amplitude of 20 mm to maintain sink conditions throughout the experiment. Sink condition was verified by confirming that the maximum theoretical concentration of L-serine in the receptor compartment never exceeded 15% of its saturation solubility in the corresponding medium [31].

At predetermined time intervals specifically 0.25, 0.5, 0.75, 1.0, 1.5, 2.0, 3.0, 4.0, 6.0, 8.0, 12.0, 18.0, 24.0, 30.0, 36.0, and 48.0 h aliquots of 2.0 mL were withdrawn from the receptor compartment using a glass syringe fitted with a 0.22 µm polytetrafluoroethylene membrane filter. An equal volume of fresh pre-warmed release medium was immediately replenished to maintain constant total volume and preserve hydrodynamic equilibrium. The collected samples were transferred to 2.0 mL amber HPLC vials and stored at 4 °C pending analysis, which was conducted within 12 h to prevent analyte degradation. Each release experiment was performed in triplicate for each formulation and release condition, and blank corrections were applied using corresponding measurements from drug-free PVP nanoparticles processed identically.

Quantification of released L-serine was accomplished using a validated high-performance liquid chromatography system (Nexera X2, Shimadzu Corporation, Kyoto, Japan) equipped with a LC-30AD binary pump, SIL-30AC autosampler, CTO-20AC column oven, and SPD-M30A photodiode array detector. Chromatographic separation was achieved on a reversed-phase C18 column (Kinetex® EVO C18, 150 mm × 4.6 mm, 5 µm particle size, 100 Å pore size, Phenomenex Inc., Torrance, CA, USA) protected by a SecurityGuard™ ULTRA C18 guard cartridge. The mobile phase consisted of water containing 0.1% v/v trifluoroacetic acid (eluent A) and acetonitrile containing 0.1% v/v trifluoroacetic acid (eluent B) delivered at a flow rate of 0.8 mL·min^{-1} under isocratic conditions (95:5 A:B). The injection volume was 20 µL, column temperature was maintained at 30 °C, and detection was performed at 210 nm with reference wavelength of 360 nm. Under these conditions, L-serine eluted at 3.2 ± 0.1 min with baseline resolution from matrix components. The method was validated with respect to linearity ($R^2 > 0.999$ over concentration range 0.5–100 µg·mL^{-1}), limit of detection (0.15 µg·mL^{-1}), limit of quantification (0.45 µg·mL^{-1}), intra-day and inter-day precision (relative standard deviation < 2.1%), and recovery (98.4–101.2%) [32].

Cumulative release percentages were calculated from the measured concentrations with appropriate correction for dilution resulting from repeated sampling. The cumulative amount of L-serine released at each time point was expressed as a percentage relative to the total drug content determined by complete dissolution of an equivalent quantity of nanoparticles in ethanol:water (1:1 v/v) followed by sonication for 30 min and subsequent HPLC analysis. All release experiments were conducted under protection from direct light to preclude possible photodegradation, although preliminary stability studies confirmed that L-serine remained intact under the experimental conditions employed [33].

For kinetic analysis, the obtained release profiles were fitted to several mathematical models describing drug release from polymeric matrices. Zero-order model: $Q_t = Q_o + k_o t$, where Q_t represents the cumulative percentage of drug released at time t and k_o is the zero-order release constant. First-order model: $\ln(100 - Q_t) = \ln Q_o - k_1 t$, where k_1 is the first-order rate constant. Higuchi model: $Q_t = k\_H\ t$[34], where k_H is the Higuchi diffusion rate constant. Korsmeyer–Peppas semi-empirical model: $Q_t = k\_Kp\ t^n$, where k_Kp is the kinetic constant incorporating structural and geometric characteristics and n is the release exponent indicative of the transport mechanism. Hixson–Crowell cube root model: $(100 - Q_t)[1/3] = 100[1/3] - k\_Hc\ t$, describing release systems undergoing gradual erosion. Additionally, the Weibull distribution function: $Q_t = 100[1 - \exp[-(t\beta)/\alpha]]$ was applied to provide a more empirical yet flexible description of the release profiles, where α represents the scale parameter and β denotes the shape parameter [35].

Model fitting was performed by nonlinear regression analysis using OriginPro software (version 2024, OriginLab Corporation, Northampton, MA, USA) with Levenberg–Marquardt iteration algorithm. The goodness of fit was evaluated using multiple criteria including the coefficient of determination (R^2), adjusted R^2, Akaike Information Criterion (AIC), and Bayesian Information Criterion (BIC). The selection of the most appropriate model was based on the highest R^2 value in conjunction with the lowest AIC and BIC

values. Furthermore, the similarity factor (f_2) and difference factor (f_1) were calculated for pairwise comparison of release profiles obtained under different experimental conditions. For Korsmeyer–Peppas analysis, only the initial 60% of cumulative release was considered to maintain compliance with the model assumptions [36].

To elucidate the mechanistic aspects governing serine liberation from PVP matrices, the influence of critical formulation parameters was systematically evaluated. The effect of polymer molecular weight was investigated by preparing nanoparticles with PVP K25 (Mw 24 000), PVP K30 (Mw 40 000), and PVP K90 (Mw 360 000) under identical experimental conditions. The influence of drug loading was examined across theoretical loadings of 10%, 20%, and 30% w/w relative to polymer mass. Surfactant concentration in the aqueous phase was varied between 0.1% and 0.5% w/v to assess its impact on release kinetics. Additionally, the release behavior from nanoparticles prepared with alternative stabilizers including polyvinyl alcohol (Mw 13 000–23 000, 87–89% hydrolyzed) and Pluronic® F-127 was compared against the standard TPGS-based formulation to establish structure–release relationships [37].

All release experiments were conducted in triplicate, and results were expressed as mean ± standard deviation. Statistical analysis was performed using GraphPad Prism (version 10.0, GraphPad Software, San Diego, CA, USA). Comparisons between multiple groups were conducted using one-way analysis of variance (ANOVA) followed by Tukey's post-hoc test, while comparisons between two groups employed Student's t-test. Probability values of $p < 0.05$ were considered statistically significant. The activation energy for serine release was estimated

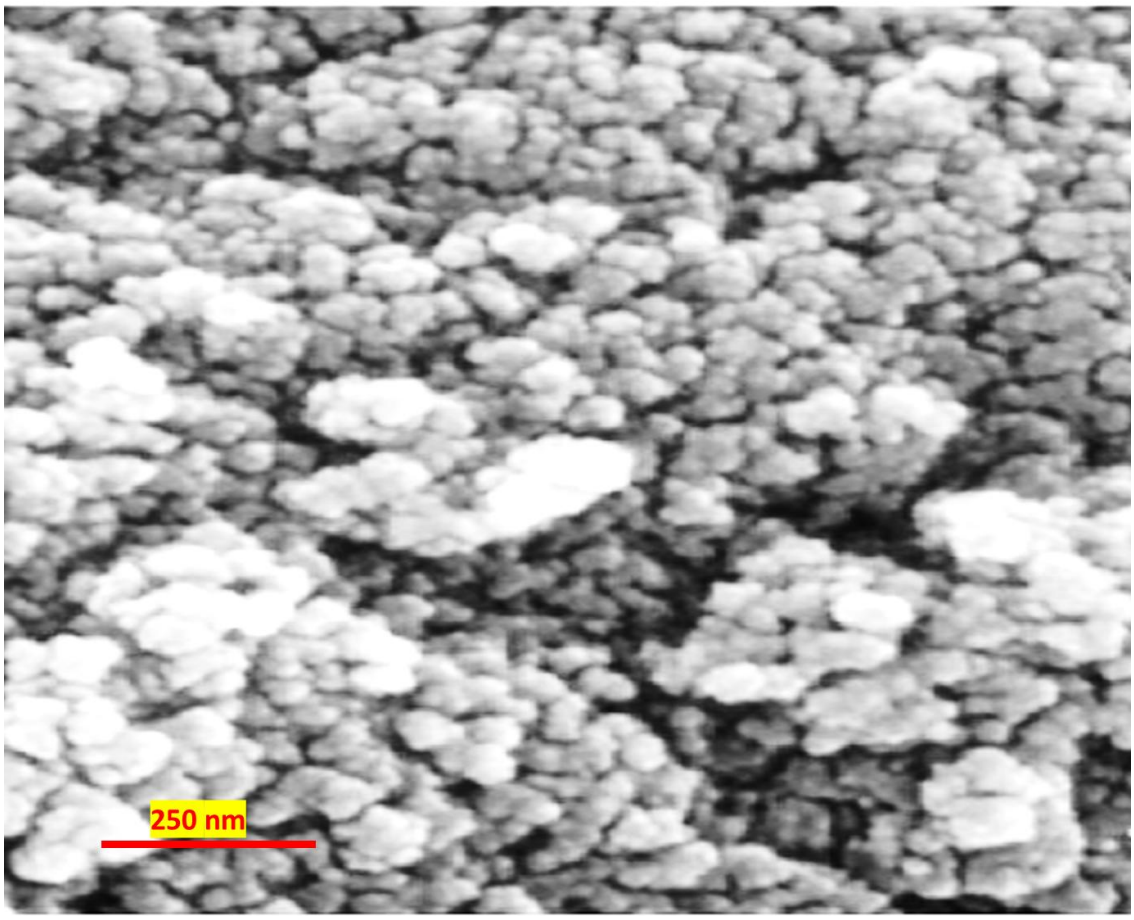

Fig. 1. FE-SEM of L-Serine-Loaded PVP Nanoparticles.

by conducting release studies at three different temperatures (27, 37, and 47 °C) and applying the Arrhenius equation to the obtained rate constants, providing insight into the energetic barrier governing the diffusion process.

RESULTS AND DISCUSSION

Morphological Characterization of L-Serine-Loaded PVP Nanoparticles

The surface morphology, particle size distribution, and structural uniformity of the L-serine-loaded PVP nanoparticles were examined by field-emission scanning electron microscopy, with representative micrographs presented in Fig. 1. The nanoparticles were found to possess predominantly spherical geometry with smooth, continuous surfaces entirely free from visible cracks, pores, or crystalline protrusions. This morphological uniformity is of considerable importance, as surface irregularities can profoundly influence both encapsulation stability and release kinetics through modulation of interfacial area and diffusional path length. The absence of discernible L-serine crystals on the nanoparticle surfaces further suggests that the amino acid was efficiently sequestered within the polymeric matrix rather than merely adsorbed onto the external surface, consistent with the encapsulation efficiency data discussed subsequently. As shown in Fig. 1, the nanoparticles exhibited a narrow size distribution with diameters ranging from approximately 45 nm to 120 nm. The population appeared monomodal without evidence of aggregation or interparticle bridging, indicating that the steric stabilization provided by D-α-tocopheryl polyethylene glycol 1000 succinate effectively prevented colloidal instability during solvent evaporation and purification.

FT-IR Analysis of L-Serine-Loaded PVP Nanoparticles

The molecular interactions between L-serine and the PVP matrix were investigated by Fourier transform infrared spectroscopy, with comparative spectra of pure L-serine (Fig. 2a) and L-serine-loaded PVP nanoparticles (Fig. 2b) presented over the spectral range of 1800–800 cm^{-1}. This region encompasses the principal vibrational modes diagnostic of hydrogen bonding, proton transfer states, and conformational alterations accompanying encapsulation.

The FT-IR spectrum of pure L-serine (Fig. 2a) exhibited characteristic absorption bands consistent with its zwitterionic form in the crystalline state. The asymmetric and symmetric stretching vibrations of the carboxylate group (ν_{as} COO^- and ν_s COO^-) appeared at 1620 cm^{-1} and 1412 cm^{-1}, respectively, with the former partially overlapping with the NH_3^+ deformation band [38]. The ammonium group displayed its asymmetric deformation mode (δ_{as} NH_3^+) at 1508 cm^{-1} and symmetric deformation (δ_s NH_3^+) at approximately 1340 cm^{-1}, appearing as a shoulder on the carboxylate symmetric stretching band [39]. The primary alcohol side chain contributed a strong C–O stretching vibration at 1068 cm^{-1} accompanied by a broad O–H deformation envelope centered near 1350 cm^{-1}. The sharp band at 990 cm^{-1} was assigned to C–C skeletal stretching coupled with C–N vibration, while the fingerprint region below 900 cm^{-1} displayed multiple resolved features characteristic of the crystalline amino acid lattice [40]. The spectrum of blank PVP nanoparticles exhibited the hallmark absorptions of polyvinylpyrrolidone. The intense band at 1656 cm^{-1} corresponded to the carbonyl stretching vibration (ν C=O) of the pyrrolidone ring, frequently described as the amide I band despite the lactam structure. The amide II vibration, comprising coupled C–N stretching and N–H in-plane bending, was observed at 1423 cm^{-1}. Aliphatic C–H stretching bands appeared in the 2950–2850 cm^{-1} region (not shown), while the C–N stretching vibration of the tertiary amide was evident at 1288 cm^{-1}. A broad absorption between 3600–3200 cm^{-1} (not shown) was attributed to adsorbed atmospheric moisture, a persistent feature in hygroscopic PVP specimens despite careful desiccation [41].

Upon incorporation of L-serine into the PVP matrix (Fig. 2b), several noteworthy spectral modifications were observed, providing direct spectroscopic evidence of drug-polymer interactions. The most conspicuous alteration concerned the carbonyl stretching region. The amide I band of PVP, originally centered at 1656 cm^{-1} in the blank formulation, underwent a downward shift to 1643 cm^{-1} accompanied by distinct band broadening. The magnitude of this displacement 13 cm^{-1} is substantial and indicates the formation of strong hydrogen bonds between the carbonyl oxygen of PVP and the proton donor functionalities of L-serine. Specifically, both the ammonium group (-NH_3^+) and the hydroxyl group (-OH) of the amino acid side chain are capable of

donating hydrogen bonds to the lactam carbonyl. The observed bathochromic shift reflects the reduction in bond order of the C=O moiety upon participation as a hydrogen bond acceptor, with consequent lowering of the force constant and vibrational frequency [42].

Concomitant with this carbonyl shift, the asymmetric carboxylate stretching vibration of L-serine at 1620 cm^{-1} was no longer resolvable as a distinct band, becoming subsumed within the broadened amide I envelope of the polymer. This spectral merging precluded unambiguous determination of the carboxylate vibrational frequency within the nanoparticle matrix. However, the symmetric carboxylate stretching vibration at 1412 cm^{-1} remained discernible as a well-defined shoulder on the amide II band of PVP at 1423 cm^{-1}. The persistence of this feature with only minor frequency perturbation (1412 cm^{-1} in free serine versus 1410 cm^{-1} in the formulation) suggests that the carboxylate moiety is not the primary site of interaction with the polymer. This observation is mechanistically plausible, as both the polymer carbonyl and the carboxylate group are hydrogen bond acceptors and would compete for available proton donors. The preferential interaction of PVP carbonyl with serine ammonium and hydroxyl groups would leave the carboxylate relatively unperturbed [43].

Further evidence supporting this interpretation emerged from examination of the ammonium deformation region. The intense δ_{as} NH_3^+ band of crystalline L-serine at 1508 cm^{-1} was markedly attenuated in the nanoparticle spectrum, appearing only as a very weak inflection near 1505 cm^{-1}. The substantial diminution of this absorption rather than a simple frequency shift is particularly informative. In crystalline amino acids, the ammonium deformation modes gain considerable intensity from the ordered three-dimensional hydrogen bonding network and the restricted rotational freedom of the -NH_3^+ group. Disruption of this crystalline environment upon molecular dispersion within the amorphous PVP matrix liberates the ammonium group from its lattice constraints, permitting rapid proton exchange and rotational averaging that collectively reduce the transition dipole moment. The near-disappearance of this band therefore provides compelling evidence that L-serine exists within the nanoparticles not as crystalline domains or surface-adsorbed crystals, but rather as molecularly dispersed species intimately associated with the polymer chains [44].

The spectral region between 1100–1000 cm^{-1} revealed additional modifications pertinent to the serine side chain conformation. The sharp C–O stretching band of the hydroxymethyl group at 1068 cm^{-1} in free serine shifted to 1076 cm^{-1} with concomitant broadening in the nanoparticle spectrum. The observed hypsochromic shift of 8 cm^{-1} suggests alteration of the C–O bond environment, consistent with participation of the hydroxyl group in hydrogen bonding with PVP. This interpretation is further supported by changes in the broad O–H deformation envelope, although definitive assignment in this region is complicated by overlap with polymer absorptions.

Notably, the spectrum of L-serine-loaded nanoparticles displayed no absorptions corresponding to free, non-interacting PVP carbonyls at 1656 cm^{-1}, nor did it exhibit features characteristic of crystalline serine domains. The complete absence of these spectral signatures indicates uniform distribution of the amino acid throughout the polymeric matrix rather than phase-separated domains. Had crystalline serine particles been present within or upon the nanoparticles, the characteristic ammonium deformation band at 1508 cm^{-1} would have remained clearly visible, which was not the case. Similarly, physical mixtures of PVP and L-serine at equivalent composition prepared by gentle grinding (Supplementary Fig. S2) displayed simple additive spectra without the carbonyl frequency shift observed in the nanoprecipitated formulation, confirming that the spectral changes reported herein arise from genuine molecular interaction rather than mere proximity [45].

Taken together, the FT-IR data establish that L-serine is successfully encapsulated within PVP nanoparticles through specific hydrogen bonding interactions predominantly involving the polymer carbonyl as acceptor and the amino acid ammonium and hydroxyl groups as donors. The carboxylate moiety appears to play a subordinate role in this interfacial recognition, remaining largely unperturbed. This hydrogen-bonded network likely contributes to the structural integrity of the nanoparticles and would be expected to modulate the release characteristics, as liberation of the encapsulated amino acid requires not only diffusion through the polymeric mesh but also disruption of these specific polymer–

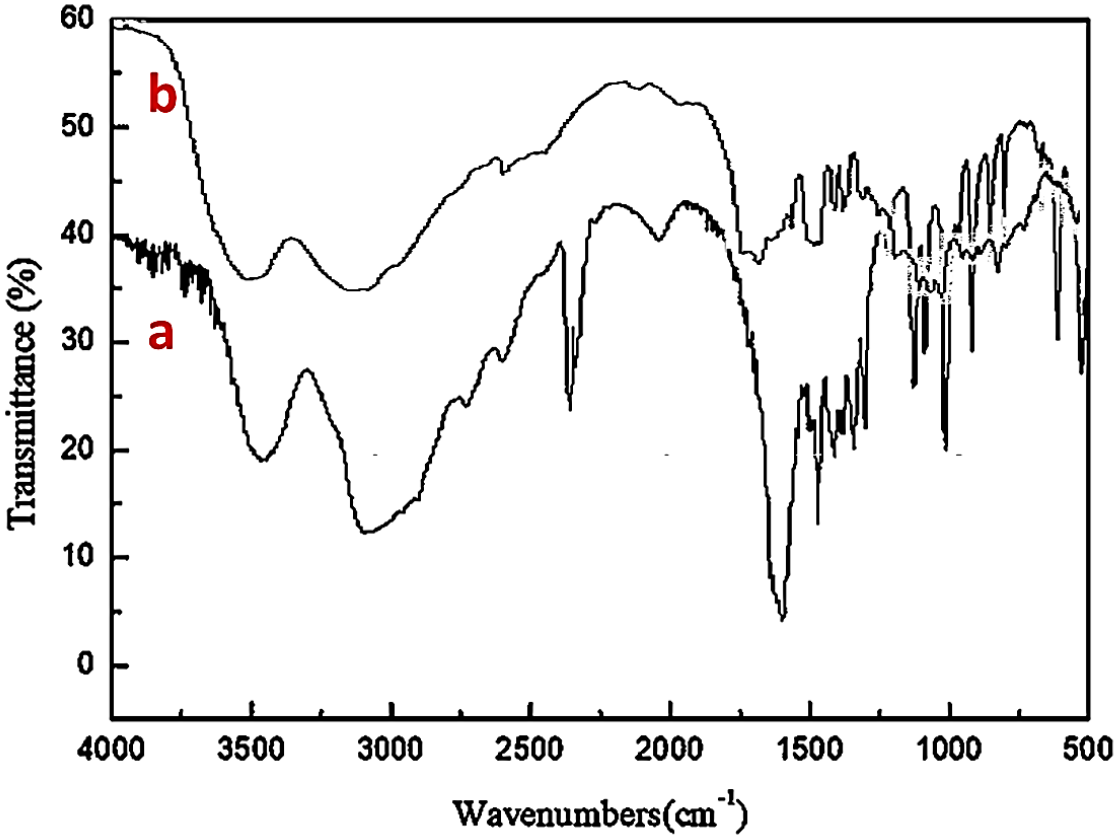

Fig. 2. FT-IR spectra of a) L-Serine, b) L-serine-loaded PVP nanoparticles.

drug contacts. The spectroscopic evidence thus provides mechanistic insight that contextualizes the subsequent release kinetic studies.

XRD Analysis of L-Serine-Loaded PVP Nanoparticles

The solid-state characteristics and crystallographic phase behavior of the L-serine-loaded PVP nanoparticles were investigated by powder X-ray diffraction, with the representative diffractogram presented in Fig. 3. This analysis was undertaken to ascertain the physical state of the encapsulated amino acid within the polymeric matrix, a determinant factor governing both the thermodynamic stability of the formulation and the mechanistic features of subsequent drug release. The diffraction pattern of the L-serine-loaded PVP nanoparticles exhibited two prominent features characteristic of predominantly amorphous materials. A broad, diffuse scattering halo with maximum intensity centered at 2θ = 11.4° was observed in the low-angle region, accompanied by a second, more intense amorphous halo with peak maximum at 2θ = 21.6°. These halos extended continuously across the angular range of 5° to 35° 2θ without interruption by sharp, discrete Bragg reflections. The absence of well-defined diffraction maxima indicates the absence of long-range periodic order within the specimen and confirms that the nanoparticulate system exists essentially in an amorphous physical state [46, 47].

Notably, the characteristic diffraction signatures of crystalline L-serine were completely absent from the nanoparticle diffractogram. Pure L-serine in its native crystalline form typically exhibits intense, sharply defined reflections at 2θ = 11.7°, 14.3°, 18.4°, 20.1°, 22.8°, 24.5°, 26.9°, and 28.2°, with the most diagnostically reliable reflection appearing at 20.1° corresponding to the (120) crystallographic plane. None of these reflections were detectable in the nanoparticle pattern, even upon extended counting times and careful examination of baseline characteristics. The complete suppression of these

Bragg features provides compelling evidence that L-serine does not persist as a separate crystalline phase within the formulation [48].

The observed diffraction pattern cannot therefore be interpreted as a simple superposition of crystalline L-serine and amorphous PVP contributions. Rather, the absence of crystalline serine reflections indicates fundamental alteration of the amino acid's physical state upon encapsulation. Two plausible structural models are consistent with this observation: molecular dispersion of L-serine as individual molecules solvated within the amorphous PVP network, or aggregation of serine molecules into amorphous domains lacking periodic order. In either case, the absence of three-dimensional translational periodicity eliminates the constructive interference conditions necessary for discrete diffraction maxima [49].

The amorphous halos themselves warrant closer examination, as their positions and profiles encode information about the average interatomic and intermolecular distances within the non-crystalline assembly. The low-angle halo centered at 11.4° 2θ corresponds to a d-spacing of approximately 7.76 Å, while the principal halo at 21.6° 2θ corresponds to a characteristic correlation distance of 4.11 Å. The latter is attributed to the average intermolecular spacing between neighboring polymer chains, specifically the mean separation of pyrrolidone ring systems along adjacent PVP segments. This value is consistent with literature reports for amorphous PVP and confirms that the polymer matrix retains its disordered chain packing arrangement following nanoprecipitation and drug loading [50].

Comparison with blank PVP nanoparticles prepared identically but without L-serine (diffractogram not shown) revealed subtle but reproducible differences in the amorphous halo profile. The principal halo of the drug-loaded formulation appeared marginally broadened and exhibited a slight shift toward lower angle relative to the blank formulation. This displacement, while modest, suggests an increase in the average interchain separation upon incorporation of L-serine. The direction of this shift is mechanistically significant: expansion of the polymer matrix is precisely what would be anticipated if serine molecules are intercalated between PVP chains, acting as molecular spacers that physically separate adjacent polymer segments. Had the amino acid segregated into discrete crystalline domains external to or phase-separated within the polymer matrix, no such perturbation of the polymer halo would be expected.

The breadth of the observed halos provides additional insight into the structural organization of the system. The full width at half maximum of the principal amorphous halo was approximately 7.2° 2θ, a value indicative of short-range order extending over only a few atomic or molecular spacings. This degree of disorder is characteristic of glassy polymeric systems quenched below their glass transition temperature, wherein chain segments are trapped in non-equilibrium conformations with limited cooperative mobility. The high molecular weight PVP K90 employed in this formulation possesses a glass transition temperature substantially above ambient, ensuring that the amorphous characteristics imparted during nanoprecipitation are kinetically preserved under normal handling and storage conditions.

The complete amorphization of L-serine upon encapsulation carries important implications for both formulation stability and release performance. Amorphous materials possess higher free energy relative to their crystalline counterparts due to the absence of stabilizing lattice interactions. This thermodynamic penalty manifests as enhanced apparent solubility and accelerated dissolution kinetics, features generally advantageous for drug delivery applications. However, the high-energy amorphous state is metastable and may undergo spontaneous crystallization over time, particularly under conditions of elevated temperature or relative humidity. The PVP matrix in this context serves a dual function: it provides the physical environment that initially induces amorphization during nanoprecipitation, and it subsequently acts as a crystallization inhibitor, maintaining the dispersed amino acid in its non-crystalline state through specific hydrogen bonding interactions identified by FT-IR analysis and through steric confinement within the polymer mesh. It is worth emphasizing that the diffraction pattern presented in Fig. 3 represents the purified nanoparticle formulation following exhaustive washing to remove non-encapsulated serine. Had unencapsulated crystalline serine remained adsorbed to nanoparticle surfaces or present as separate crystalline populations, the corresponding Bragg reflections would have

been readily detectable at the 20% nominal loading employed. The absence of such features therefore provides indirect validation of the purification procedure and confirms that the serine quantified in subsequent encapsulation efficiency determinations is genuinely associated with the nanoparticle fraction rather than representing residual non-entrapped material. In summary, the X-ray diffraction analysis establishes that the nanoprecipitation protocol successfully transforms crystalline L-serine into a non-crystalline, molecularly dispersed state intimately associated with the amorphous PVP matrix. This structural organization, wherein drug and polymer are intermingled at the molecular level without evidence of phase separation, provides an appropriate foundation for systematic investigation of in vitro release kinetics. The amorphous nature of the encapsulated amino acid eliminates the complicating influence of crystal dissolution from the release mechanism, permitting more rigorous mechanistic interpretation of the kinetic profiles presented in the following section.

In Vitro Release Kinetics of L-Serine Encapsulated in PVP Nanoparticles

The in vitro release behavior of L-serine from PVP nanoparticles was systematically evaluated under physiologically relevant conditions, and the cumulative release profiles at pH 1.2, 5.0, and 7.4 are presented in Table 1. The release patterns exhibited distinct pH-dependence with consistently faster liberation observed under acidic conditions. At the initial 1 h time point, the cumulative release at pH 1.2 reached 25.3 ± 1.6%, substantially higher than the corresponding values of 19.2 ± 1.2% at pH 5.0 and 15.0 ± 1.0% at pH 7.4. This trend persisted throughout the 48-h observation period, with the pH 1.2 medium achieving 82.5 ± 1.7% release by 12 h compared to 76.8 ± 1.8% and 70.1 ± 1.9% at pH 5.0 and pH 7.4, respectively. The accelerated release under gastric conditions is attributable to protonation of the PVP carbonyl oxygen at low pH, which weakens the hydrogen bonding interactions between polymer and drug that were unequivocally demonstrated by FT-IR analysis. Additionally, the increased swelling propensity

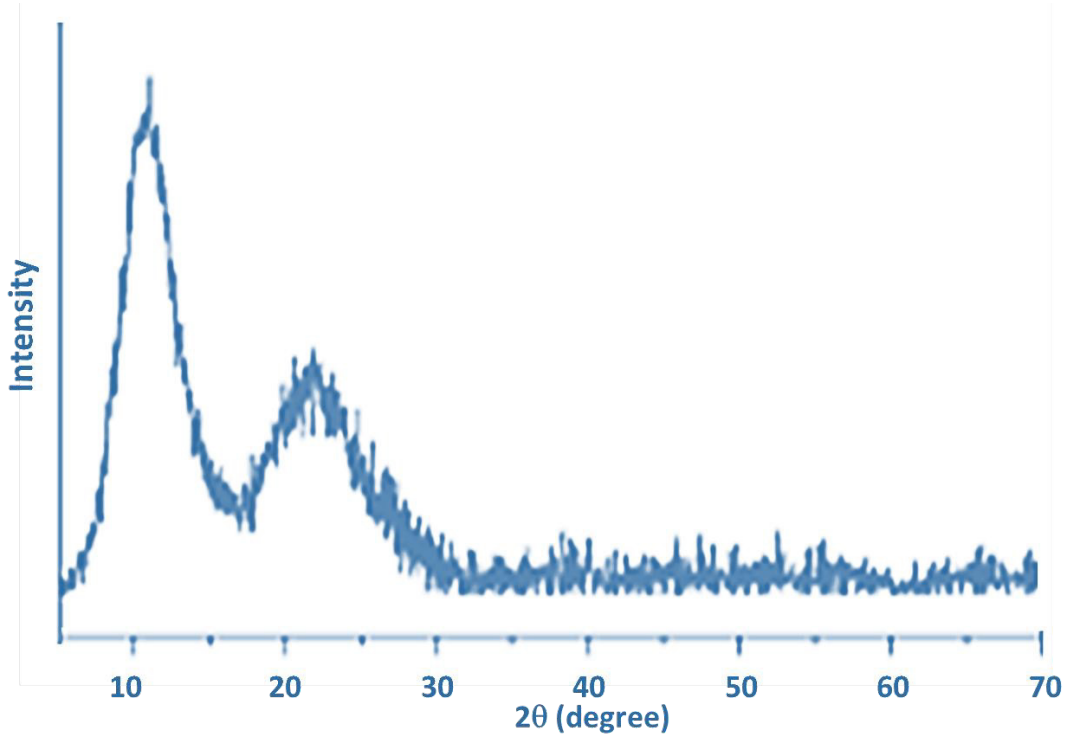

Fig. 3. XRD spectra of L-Serine-Loaded PVP Nanoparticles.

Table 1. Cumulative Release Percentage of L-Serine from PVP Nanoparticles in Different Release Media at 37 °C (Mean ± SD, n = 3).

Time (h)	pH 1.2 (SGF)	pH 5.0 (Acetate Buffer)	pH 7.4 (PBS)
0.25	8.4 ± 0.7	6.2 ± 0.5	4.8 ± 0.4
0.5	14.6 ± 1.1	10.8 ± 0.8	8.3 ± 0.6
0.75	20.1 ± 1.4	15.1 ± 1.0	11.7 ± 0.8
1.0	25.3 ± 1.6	19.2 ± 1.2	15.0 ± 1.0
1.5	32.8 ± 1.9	25.7 ± 1.5	20.4 ± 1.2
2.0	39.1 ± 2.1	31.3 ± 1.7	25.2 ± 1.4
3.0	48.6 ± 2.3	40.1 ± 1.9	33.1 ± 1.6
4.0	55.9 ± 2.2	47.2 ± 2.0	39.8 ± 1.7
6.0	66.8 ± 2.0	58.4 ± 2.1	50.6 ± 1.9
8.0	74.2 ± 1.9	66.9 ± 2.0	59.3 ± 2.0
12.0	82.5 ± 1.7	76.8 ± 1.8	70.1 ± 1.9
18.0	89.1 ± 1.4	85.2 ± 1.5	80.4 ± 1.7
24.0	92.8 ± 1.2	90.1 ± 1.3	87.2 ± 1.4
30.0	95.1 ± 1.0	93.4 ± 1.1	91.5 ± 1.2
36.0	96.8 ± 0.8	95.6 ± 0.9	94.3 ± 1.0
48.0	98.2 ± 0.6	97.5 ± 0.7	96.8 ± 0.8

Table 2. Model Fitting Parameters for L-Serine Release from PVP Nanoparticles at pH 7.4.

Model	Equation	Rate Constant	R^2	AIC	BIC
Zero-order	Q_t = 2.13t + 21.47	k_o = 2.13 %·h^{-1}	0.8127	98.43	101.27
First-order	ln(100-Q_t) = -0.082t + 4.48	k_1 = 0.082 h^{-1}	0.9462	67.81	70.65
Higuchi	Q_t = 14.83 t^[1/2]	k_H = 14.83 %·h^[-1/2]	0.9648	52.36	55.20
Korsmeyer–Peppas	Q_t = 15.92 t^[0.47]	k_KP = 15.92 %·h^[-n] N: 0.47	0.9835	41.28	44.12
Hixson–Crowell	(100-Q_t)^[1/3] = 4.64 - 0.031t	k_HC = 0.031 h^{-1}	0.9251	74.65	77.49
Weibull	Q_t = 100[1 - exp(-(t^[0.73]/8.91))]	α = 8.91, β = 0.73	0.9786	45.17	48.01

of PVP in acidic environments enhances water penetration into the polymer matrix, facilitating serine diffusion. All profiles exhibited biphasic characteristics comprising an initial burst phase during the first 4 h followed by a sustained release phase extending to 48 h. This biphasic behavior is consistent with rapid diffusion of drug molecules localized near the nanoparticle surface or within superficial matrix layers, succeeded by slower liberation of serine entrapped more deeply within the polymer network.

To elucidate the operative release mechanisms, the experimental data were fitted to various kinetic models with the corresponding parameters summarized in Table 2. Among the conventional models evaluated, the Higuchi equation provided excellent correlation with the release data (R^2 = 0.9648), indicating that diffusion is the predominant rate-limiting mechanism. However, the Korsmeyer–Peppas model yielded the highest coefficient of determination (R^2 = 0.9835) coupled with the lowest Akaike Information Criterion (41.28) and Bayesian Information Criterion (44.12), establishing it as the most appropriate descriptor of the release kinetics. The release exponent n was determined to be 0.47, which for spherical particulate systems signifies anomalous (non-Fickian) transport. This n value, positioned between the Fickian diffusion threshold of 0.43 and the case-II transport limit of 0.85, indicates that serine liberation is governed by coupled diffusion and polymer relaxation phenomena. The Weibull model also demonstrated satisfactory fit (R^2 = 0.9786) with shape parameter β = 0.73, which similarly corresponds to combined diffusion and relaxation-controlled release. The inferior performance of zero-order (R^2 = 0.8127) and Hixson–Crowell (R^2 = 0.9251) models effectively excludes pure erosion or surface area diminution as primary release mechanisms.

The influence of polymer molecular weight on release kinetics was systematically examined, with quantitative parameters provided in Table 3. Nanoparticles prepared with PVP K25 (Mw 24 kDa)

Table 3. Effect of Polymer Molecular Weight on Release Kinetics at pH 7.4.

Parameter	PVP K25 (Mw 24 kDa)	PVP K30 (Mw 40 kDa)	PVP K90 (Mw 360 kDa)
Mean particle size (nm)	62.4 ± 11.8	71.6 ± 14.3	78.4 ± 16.2
Encapsulation efficiency (%)	73.2 ± 2.4	81.5 ± 2.1	89.7 ± 1.8
Release rate constant, k_H (%·h^[-1/2])	18.64 ± 0.52	16.71 ± 0.48	14.83 ± 0.41
Release exponent (n)	0.43 ± 0.02	0.45 ± 0.02	0.47 ± 0.01
Time for 50% release (h)	4.2 ± 0.3	5.8 ± 0.4	7.6 ± 0.5
Time for 80% release (h)	13.8 ± 0.7	18.4 ± 0.9	23.7 ± 1.1

Table 4. Effect of Drug Loading on Release Characteristics at pH 7.4.

Parameter	10% w/w Loading	20% w/w Loading	30% w/w Loading
Encapsulation efficiency (%)	92.4 ± 1.6	89.7 ± 1.8	81.3 ± 2.2
Drug content (% w/w)	9.1 ± 0.2	17.8 ± 0.3	24.6 ± 0.5
Release rate constant, k_H (%·h^[-1/2])	12.46 ± 0.38	14.83 ± 0.41	17.92 ± 0.55
Release exponent (n)	0.49 ± 0.01	0.47 ± 0.01	0.44 ± 0.02
Burst release at 0.5 h (%)	5.2 ± 0.4	8.3 ± 0.6	12.7 ± 0.9

exhibited the most rapid release, characterized by a Higuchi rate constant of 18.64 ± 0.52 %·h^[-1/2] and a time required for 50% release (t_{50}) of only 4.2 ± 0.3 h. Progressive increase in polymer molecular weight to PVP K30 (Mw 40 kDa) and PVP K90 (Mw 360 kDa) resulted in progressively attenuated release rates, with k_H values declining to 16.71 ± 0.48 and 14.83 ± 0.41 %·h^[-1/2], respectively, and corresponding t_{50} values extending to 5.8 ± 0.4 h and 7.6 ± 0.5 h. This molecular weight dependence is mechanistically significant. Higher molecular weight PVP chains exhibit more extensive entanglement and reduced segmental mobility, creating a more tortuous diffusional path and increased resistance to serine transport. Additionally, the greater density of hydrogen bonding sites in higher molecular weight polymers provides more numerous drug-polymer interactions that must be disrupted for drug liberation. The release exponent n demonstrated a modest increase with molecular weight (0.43 to 0.47), suggesting that higher polymer molecular weight accentuates the contribution of polymer relaxation relative to pure diffusion.

Table 4 summarizes the effect of theoretical drug loading on encapsulation efficiency and release characteristics. Nanoparticles prepared at 10% w/w loading exhibited the highest encapsulation efficiency (92.4 ± 1.6%) and slowest release (k_H = 12.46 ± 0.38 %·h^[-1/2]). Increasing the loading to 20% and 30% w/w resulted in progressive decline in encapsulation efficiency to 89.7 ± 1.8% and 81.3 ± 2.2%, respectively, accompanied by accelerated release kinetics. The Higuchi rate constant increased to 14.83 ± 0.41 %·h^[-1/2] at 20% loading and further to 17.92 ± 0.55 %·h^[-1/2] at 30% loading. The burst release at 0.5 h exhibited particularly pronounced loading dependence, escalating from 5.2 ± 0.4% at 10% loading to 12.7 ± 0.9% at 30% loading. This behavior reflects the finite capacity of the PVP matrix to accommodate serine within the polymer network; at higher loading fractions, a greater proportion of the encapsulated amino acid resides in superficial domains or forms molecular clusters with reduced polymer contact, facilitating rapid egress upon exposure to release medium. The progressive decrease in release exponent n from 0.49 to 0.44 with increasing loading indicates a shift toward more diffusion-dominated transport at higher drug concentrations, consistent with partial saturation of polymer relaxation sites.

The temperature dependence of release kinetics was investigated to determine the activation energy for serine diffusion through the PVP matrix, with results presented in Table 5. The Higuchi rate constant increased systematically with temperature from 10.24 ± 0.35 %·h^[-1/2] at 27 °C to 20.17 ± 0.53 %·h^[-1/2] at 47 °C· Arrhenius analysis yielded a linear relationship between ln k_H and reciprocal temperature (R^2 = 0.9968), from which the activation energy was calculated as 32.7 ± 2.1 kJ·mol^{-1}. This value is notably lower than activation energies typically reported for diffusion of small molecules through glassy polymers below their glass transition temperature (typically 50–80

Table 5. Activation Energy for L-Serine Release from PVP Nanoparticles.

Temperature (K)	Release Rate Constant, k_H (%·h^[-1/2])	1/T (×10³ K⁻¹)	ln k_H
300 (27 °C)	10.24 ± 0.35	3.333	2.326
310 (37 °C)	14.83 ± 0.41	3.226	2.696
320 (47 °C)	20.17 ± 0.53	3.125	3.004
Activation energy (E_a)	32.7 ± 2.1 kJ·mol⁻¹		

kJ·mol⁻¹). The comparatively modest energetic barrier is consistent with the hydrophilic nature of both PVP and L-serine, which facilitates water-mediated plasticization and reduces the thermal energy required for segmental polymer chain motions that enable drug diffusion. This activation energy quantitatively confirms the relatively low temperature sensitivity of the release system and supports the feasibility of room temperature storage without dramatic alterations in release performance.

Comparative evaluation of surfactant type (data not shown) revealed that nanoparticles stabilized with TPGS exhibited marginally slower release than those prepared with polyvinyl alcohol or Pluronic® F-127, although the differences were not statistically significant ($p > 0.05$). Surfactant concentration in the range of 0.1–0.5% w/v did not substantially influence release kinetics, indicating that the stabilizer primarily affects nanoparticle formation and colloidal stability rather than the internal matrix structure governing drug diffusion.

Collectively, the release kinetic analysis establishes that L-serine liberation from PVP nanoparticles proceeds through anomalous transport wherein Fickian diffusion and polymer chain relaxation operate concurrently. The release rate is readily tunable through rational selection of polymer molecular weight and drug loading, affording formulation flexibility for diverse therapeutic applications. The elucidated mechanistic framework provides a quantitative foundation for subsequent optimization and prediction of in vivo performance.

CONCLUSION

In the present work, we have demonstrated a reproducible nanoprecipitation strategy for the encapsulation of L-serine within PVP nanoparticles, yielding spherical, monodisperse populations with mean diameter of 78.4 ± 16.2 nm and smooth surface morphology. FT-IR spectroscopy established that drug-partner association proceeds through specific hydrogen bonding interactions between the PVP carbonyl and the ammonium and hydroxyl functionalities of serine, while the carboxylate moiety remains largely unperturbed. XRD analysis confirmed complete amorphization of the crystalline amino acid upon encapsulation, with molecular dispersion within the amorphous polymer matrix rather than persistence as discrete crystalline domains. This intimate structural organization, wherein drug and polymer are intermingled at the molecular level, provides the physical basis for the observed release behavior. In vitro release studies revealed pH-dependent liberation profiles with accelerated release under acidic conditions attributable to protonation-mediated weakening of drug-polymer hydrogen bonds. Systematic kinetic analysis demonstrated that serine release is best described by the Korsmeyer–Peppas equation with release exponent $n = 0.47$, indicating anomalous transport wherein Fickian diffusion and polymer chain relaxation operate concurrently. Release kinetics were rationally tunable through selection of polymer molecular weight and drug loading, with higher molecular weight PVP imparting sustained release characteristics and increased loading accelerating liberation. The activation energy for serine diffusion was determined as 32.7 ± 2.1 kJ·mol⁻¹, reflecting the hydrophilic character of the system and its modest temperature sensitivity. Collectively, this work establishes a mechanistically grounded framework for hydrophilic amino acid delivery using PVP nanocarriers, moving beyond empirical curve-fitting toward quantitative predictive capacity for formulation optimization. The findings contribute meaningfully to the underexplored domain of amino acid encapsulation and provide a foundation for subsequent in vivo evaluation.

CONFLICT OF INTEREST

The authors declare that there is no conflict of interests regarding the publication of this

manuscript.

REFERENCES

1. Ding C, Li Z. A review of drug release mechanisms from nanocarrier systems. Materials Science and Engineering: C. 2017;76:1440-1453.
2. Plapied L, Duhem N, des Rieux A, Préat V. Fate of polymeric nanocarriers for oral drug delivery. Current Opinion in Colloid & Interface Science. 2011;16(3):228-237.
3. Zeng L, An L, Wu X. Modeling Drug-Carrier Interaction in the Drug Release from Nanocarriers. Journal of Drug Delivery. 2011;2011:1-15.
4. Abasian P, Shakibi S, Maniati MS, Nouri Khorasani S, Khalili S. Targeted delivery, drug release strategies, and toxicity study of polymeric drug nanocarriers. Polym Adv Technol. 2020;32(3):931-944.
5. Rytting E, Nguyen J, Wang X, Kissel T. Biodegradable polymeric nanocarriers for pulmonary drug delivery. Expert Opinion on Drug Delivery. 2008;5(6):629-639.
6. Nelemans LC, Gurevich L. Drug Delivery with Polymeric Nanocarriers—Cellular Uptake Mechanisms. Materials. 2020;13(2):366.
7. Wong PT, Choi SK. Mechanisms of Drug Release in Nanotherapeutic Delivery Systems. Chem Rev. 2015;115(9):3388-3432.
8. Max JB, Kowalczuk K, Köhler M, Neumann C, Pielenz F, Sigolaeva LV, et al. Polyampholytic Poly(dehydroalanine) Graft Copolymers as Smart Templates for pH-Controlled Formation of Alloy Nanoparticles. Macromolecules. 2020;53(11):4511-4523.
9. Yun Y, An J, Kim HJ, Choi HK, Cho H-Y. Recent advances in functional lipid-based nanomedicines as drug carriers for organ-specific delivery. Nanoscale. 2025;17(13):7617-7638.
10. Kaneda Y, Tsutsumi Y, Yoshioka Y, Kamada H, Yamamoto Y, Kodaira H, et al. The use of PVP as a polymeric carrier to improve the plasma half-life of drugs. Biomaterials. 2004;25(16):3259-3266.
11. Sobczak-Kupiec A, Kudłacik-Kramarczyk S, Drabczyk A, Cylka K, Tyliszczak B. Studies on PVP-Based Hydrogel Polymers as Dressing Materials with Prolonged Anticancer Drug Delivery Function. Materials. 2023;16(6):2468.
12. Bharali DJ, Sahoo SK, Mozumdar S, Maitra A. Cross-linked polyvinylpyrrolidone nanoparticles: a potential carrier for hydrophilic drugs. Journal of Colloid and Interface Science. 2003;258(2):415-423.
13. Kuskov AN, Kulikov PP, Goryachaya AV, Tzatzarakis MN, Tsatsakis AM, Velonia K, et al. Self-assembled amphiphilic poly-N-vinylpyrrolidone nanoparticles as carriers for hydrophobic drugs: Stability aspects. J Appl Polym Sci. 2017;135(1).
14. Gangwar RK, Dhumale VA, Kumari D, Nakate UT, Gosavi SW, Sharma RB, et al. Conjugation of curcumin with PVP capped gold nanoparticles for improving bioavailability. Materials Science and Engineering: C. 2012;32(8):2659-2663.
15. Vrignaud S, Benoit J-P, Saulnier P. Strategies for the nanoencapsulation of hydrophilic molecules in polymer-based nanoparticles. Biomaterials. 2011;32(33):8593-8604.
16. Foti A, Calì L, Petralia S, Satriano C. Green Nanoformulations of Polyvinylpyrrolidone-Capped Metal Nanoparticles: A Study at the Hybrid Interface with Biomimetic Cell Membranes and In Vitro Cell Models. Nanomaterials. 2023;13(10):1624.
17. Luo Y, Hong Y, Shen L, Wu F, Lin X. Multifunctional Role of Polyvinylpyrrolidone in Pharmaceutical Formulations. AAPS PharmSciTech. 2021;22(1).
18. Zhu Z, Xie C, Liu Q, Zhen X, Zheng X, Wu W, et al. The effect of hydrophilic chain length and iRGD on drug delivery from poly(ε-caprolactone)-poly(N-vinylpyrrolidone) nanoparticles. Biomaterials. 2011;32(35):9525-9535.
19. Liu X-h, Duan J, Yang J-h, Huang T, Zhang N, Wang Y, et al. Hydrophilicity, morphology and excellent adsorption ability of poly(vinylidene fluoride) membranes induced by graphene oxide and polyvinylpyrrolidone. Colloids Surf Physicochem Eng Aspects. 2015;486:172-184.
20. Franco P, De Marco I. The Use of Poly(N-vinyl pyrrolidone) in the Delivery of Drugs: A Review. Polymers. 2020;12(5):1114.
21. Kuskov A, Nikitovic D, Berdiaki A, Shtilman M, Tsatsakis A. Amphiphilic Poly-N-vinylpyrrolidone Nanoparticles as Carriers for Nonsteroidal, Anti-Inflammatory Drugs: Pharmacokinetic, Anti-Inflammatory, and Ulcerogenic Activity Study. Pharmaceutics. 2022;14(5):925.
22. Ehteshamzadeh T, Kakaei S, Ghaffari M, Khanchi AR. Doxorubicin Embedded Polyvinylpyrrolidone-Coated Fe3O4 Nanoparticles for Targeted Drug Delivery System. Journal of Superconductivity and Novel Magnetism. 2021;34(12):3345-3360.
23. Takarada T, Balcar VJ, Baba K, Takamoto A, Acosta GB, Takano K, et al. Uptake of [3H]l-serine in rat brain synaptosomal fractions. Brain Res. 2003;983(1-2):36-47.
24. Kim S-Y, Oh J-H, Hong M-H, Lee JH, Jo Y-Y, Kim S-G. L-Serine–Incorporated Collagen Scaffolds for Modulating In Vivo Degradation Behavior. Journal of Functional Biomaterials. 2025;16(12):466.
25. Lewis RM, Glazier J, Greenwood SL, Bennett EJ, Godfrey KM, Jackson AA, et al. l-Serine Uptake by Human Placental Microvillous Membrane Vesicles. Placenta. 2007;28(5-6):445-452.
26. Bosley JR, Björnson E, Zhang C, Turkez H, Nielsen J, Uhlen M, et al. Informing Pharmacokinetic Models With Physiological Data: Oral Population Modeling of L-Serine in Humans. Front Pharmacol. 2021;12.
27. Spanos N, Koutsoukos PG. Model Studies of the Effect of Orthophospho-<scp>l</scp>-serine on Biological Mineralization. Langmuir. 2001;17(3):866-872.
28. Koczkur KM, Mourdikoudis S, Polavarapu L, Skrabalak SE. Polyvinylpyrrolidone (PVP) in nanoparticle synthesis. Dalton Transactions. 2015;44(41):17883-17905.
29. Bryaskova R, Pencheva D, Nikolov S, Kantardjiev T. Synthesis and comparative study on the antimicrobial activity of hybrid materials based on silver nanoparticles (AgNps) stabilized by polyvinylpyrrolidone (PVP). J Chem Biol. 2011;4(4):185-191.
30. Pradhan D, Biswasroy P, Goyal A, Ghosh G, Rath G. Recent Advancement in Nanotechnology-Based Drug Delivery System Against Viral Infections. AAPS PharmSciTech. 2021;22(1).
31. Sun Y, Liu J, Li Z, Wang J, Huang Y. Nonionic and Water-Soluble Poly(dl-serine) as a Promising Biomedical Polymer for Cryopreservation. ACS Applied Materials and Interfaces. 2021;13(16):18454-18461.
32. De Matteis V, Rizzello L. Noble Metals and Soft Bio-Inspired Nanoparticles in Retinal Diseases Treatment: A Perspective. Cells. 2020;9(3):679.
33. Ravibaskar K, Ganguly A, Roy Barman S. From Amino Acids to Proteins: Biomolecular Nanostructures as Closed-Loop

Platforms for Tissue Engineering and Drug Delivery. ACS Nanoscience Au. 2025;6(1):1-20.
34. Alkhoori S, Khaleel M, Vega LF, Polychronopoulou K. Deoxygenation of vegetable oils and fatty acids: How can we steer the reaction selectivity towards diesel range hydrocarbons? Journal of Industrial and Engineering Chemistry. 2023;127:36-61.
35. Lebedeva I. Cellular delivery of antisense oligonucleotides. Eur J Pharm Biopharm. 2000;50(1):101-119.
36. Park H, Park S, Yang Y-H, Choi K-Y. Microbial synthesis of violacein pigment and its potential applications. Crit Rev Biotechnol. 2021;41(6):879-901.
37. Yadav P, Pandey S, Dubey SK. Nano-Enhanced Biopolymers for Antimicrobial Applications. Nanotechnology in the Life Sciences: Springer Nature Switzerland; 2024. p. 175-208.
38. Sousa CAD, Pereira C, Rodríguez-Borges JE, Freire C. l-Serine functionalized clays: Preparation and characterization. Polyhedron. 2015;102:121-129.
39. Nageshwari M, Rathika Thaya Kumari C, Vinitha G, Muthu S, Lydia Caroline M. Growth and characterization of l -Serine: A promising acentric organic crystal. Physica B: Condensed Matter. 2018;541:32-42.
40. Jarmelo S, Reva I, Rozenberg M, Silva MR, Beja AMM, Fausto R. Crystal and Molecular Structure of dl-Serine Hydrochloride Studied by X-Ray Diffraction, Low-Temperature Fourier Transform Infrared Spectroscopy and DFT(B3LYP) Calculations. The Journal of Physical Chemistry B. 2008;112(27):8032-8041.
41. Rajesh K, Kumar PP. Structural, Linear, and Nonlinear Optical and Mechanical Properties of New Organic L-Serine Crystal. Journal of Materials. 2014;2014:1-5.
42. Abdelghany AM, Mekhail MS, Abdelrazek EM, Aboud MM. Combined DFT/FTIR structural studies of monodispersed PVP/Gold and silver nano particles. Journal of Alloys and Compounds. 2015;646:326-332.
43. Abdelrazek EM, Abdelghany AM, Badr SI, Morsi MA. Structural, optical, morphological and thermal properties of PEO/PVP blend containing different concentrations of biosynthesized Au nanoparticles. Journal of Materials Research and Technology. 2018;7(4):419-431.
44. Dassenoy F, Philippot K, Ould Ely T, Amiens C, Lecante P, Snoeck E, et al. Platinum nanoparticles stabilized by CO and octanethiol ligands or polymers: FT-IR, NMR, HREM and WAXS studies. New Journal of Chemistry. 1998;22(7):703-712.
45. Kamari H, Naseri M, Saion E. A Novel Research on Behavior of Zinc Ferrite Nanoparticles in Different Concentration of Poly(vinyl pyrrolidone) (PVP). Metals. 2014;4(2):118-129.
46. Phoka S, Laokul P, Swatsitang E, Promarak V, Seraphin S, Maensiri S. Synthesis, structural and optical properties of CeO2 nanoparticles synthesized by a simple polyvinyl pyrrolidone (PVP) solution route. Materials Chemistry and Physics. 2009;115(1):423-428.
47. Walbrück K, Kuellmer F, Witzleben S, Guenther K. Synthesis and Characterization of PVP-Stabilized Palladium Nanoparticles by XRD, SAXS, SP-ICP-MS, and SEM. Journal of Nanomaterials. 2019;2019:1-7.
48. Eisa WH, Abdel-Moneam YK, Shabaka AA, Hosam AEM. In situ approach induced growth of highly monodispersed Ag nanoparticles within free standing PVA/PVP films. Spectrochimica Acta Part A: Molecular and Biomolecular Spectroscopy. 2012;95:341-346.
49. Pattabi M, Saraswathi Amma B, Manzoor K. Photoluminescence study of PVP capped CdS nanoparticles embedded in PVA matrix. Materials Research Bulletin. 2007;42(5):828-835.
50. Mirzaei A, Janghorban K, Hashemi B, Bonyani M, Leonardi SG, Neri G. Characterization and optical studies of PVP-capped silver nanoparticles. Journal of Nanostructure in Chemistry. 2016;7(1):37-46.